Am J Physiol Endocrinol Metab 316: E96–E105, 2019.
First published November 20, 2018; doi:10.1152/ajpendo.00265.2018.

RESEARCH ARTICLE

The effect of PPARγ inhibition on bone marrow adipose tissue and bone in C3H/HeJ mice

Kerensa M. Beekman,[1,2] Annegreet G. Veldhuis-Vlug,[3] Albert van der Veen,[4,5] Martin den Heijer,[1] Mario Maas,[2] Greet Kerckhofs,[6,7,8] Tatjana N. Parac-Vogt,[9] Peter H. Bisschop,[3]* and Nathalie Bravenboer[10,11]*

[1]*Amsterdam Movement Sciences, Section of Endocrinology, Department of Internal Medicine, Vrije Universiteit, Amsterdam University Medical Center, Amsterdam, The Netherlands;* [2]*Amsterdam Movement Sciences, Department of Radiology and Nuclear Medicine, University of Amsterdam, Amsterdam University Medical Center, Amsterdam, The Netherlands;* [3]*Amsterdam Movement Sciences, Department of Endocrinology and Metabolism, University of Amsterdam, Amsterdam University Medical Center, Amsterdam, The Netherlands;* [4]*Department of Physics and Medical Technology, Vrije Universiteit, Amsterdam University Medical Center, Amsterdam, The Netherlands;* [5]*Department Cardiology, Vrije Universiteit, Amsterdam University Medical Center, Amsterdam, The Netherlands;* [6]*Biomechanics Laboratory, Institute of Mechanics, Materials, and Civil Engineering, Université Catholique de Louvain, Louvain-la-Neuve, Belgium;* [7]*Department Materials Engineering, KU Leuven, Leuven, Belgium;* [8]*Prometheus, Division of Skeletal Tissue Engineering, KU Leuven, Leuven, Belgium;* [9]*Laboratory of Bioinorganic Chemistry, Chemistry Department, KU Leuven, Leuven, Belgium;* [10]*Amsterdam Movement Sciences, Research Laboratory Bone and Calcium Metabolism, Department of Clinical Chemistry, Vrije Universiteit, Amsterdam University Medical Center, Amsterdam, The Netherlands; and* [11]*Department of Internal Medicine, Leiden University Medical Center, Leiden, The Netherlands*

Submitted 2 July 2018; accepted in final form 18 November 2018

Beekman KM, Veldhuis-Vlug AG, van der Veen A, den Heijer M, Maas M, Kerckhofs G, Parac-Vogt TN, Bisschop PH, Bravenboer N. The effect of PPARγ inhibition on bone marrow adipose tissue and bone in C3H/HeJ mice. *Am J Physiol Endocrinol Metab* 316: E96–E105, 2019. First published November 20, 2018; doi: 10.1152/ajpendo.00265.2018.—Bone marrow adipose tissue (BMAT) increases after menopause, and increased BMAT is associated with osteoporosis and prevalent vertebral fractures. Peroxisome proliferator-activated receptor-γ (PPARγ) activation promotes adipogenesis and inhibits osteoblastogenesis; therefore, PPARγ is a potential contributor to the postmenopausal increase in BMAT and decrease in bone mass. The aim of this study is to determine if PPARγ inhibition can prevent ovariectomy-induced BMAT increase and bone loss in C3H/HeJ mice. Fourteen-week-old female C3H/HeJ mice ($n = 40$) were allocated to four intervention groups: sham surgery (Sham) or ovariectomy (OVX; isoflurane anesthesia) with either vehicle (Veh) or PPARγ antagonist administration (GW9662; 1 $mg \cdot kg^{-1} \cdot day^{-1}$, daily intraperitoneal injections) for 3 wk. We measured BMAT volume, adipocyte size, adipocyte number. and bone structural parameters in the proximal metaphysis of the tibia using polyoxometalate-based contrast enhanced-nanocomputed topogaphy. Bone turnover was measured in the contralateral tibia using histomorphometry. The effects of surgery and treatment were analyzed by two-way ANOVA. OVX increased the BMAT volume fraction (Sham + Veh: 2.9 ± 2.7% vs. OVX + Veh: 8.1 ± 5.0%: $P < 0.001$), average adipocyte diameter (Sham + Veh: 19.3 ± 2.6 μm vs. OVX + Veh: 23.1 ± 3.4 μm: $P = 0.001$), and adipocyte number (Sham + Veh: 584 ± 337cells/μm^3 vs. OVX + Veh: 824 ± 113cells/μm^3: $P = 0.03$), while OVX decreased bone volume fraction (Sham + Veh: 15.5 ± 2.8% vs. OVX + Veh: 7.7 ± 1.9%; $P < 0.001$). GW9662 had no effect on BMAT, bone structural parameters, or bone turnover. In conclusion, ovariectomy increased BMAT and decreased bone volume in C3H/HeJ mice. The PPARγ antagonist GW9662 had no effect on BMAT or bone volume in C3H/HeJ mice, suggesting that BMAT accumulation is regulated independently of PPARγ in C3H/HeJ mice.

bone marrow adipose tissue; bone turnover; C3H/HeJ mice; ovariectomy; PPARγ antagonist

INTRODUCTION

Osteoporosis along with its associated risk of fractures is an increasing problem in our aging society. High marrow fat has often been associated with low bone volume and osteoporosis (11, 18, 20), as well as with prevalent vertebral fractures (38, 45), even independently of bone mineral density in some studies (7, 39). Estrogen treatment can decrease bone marrow adipose tissue (BMAT) (25) by decreasing adipocyte size and adipocyte number (41) and increase bone mineral density (BMD) in postmenopausal osteoporosis (26). However, estrogen treatment is not recommended for long-term treatment of osteoporosis due to increased risk of breast cancer and thrombosis (12, 17).

Osteoblasts and bone marrow adipocytes are both derived from skeletal stem cells (SSCs; also known as mesenchymal stromal cells) (31, 42). The lineage fate of SSCs is determined by several factors, including peroxisome proliferator-activated receptor-γ (PPARγ). PPARγ is part of the nuclear receptor superfamily and is activated by endogenous ligands such as fatty acids and exogenous ligands such as thiazolidinediones (33, 36). PPARγ exist in two isoforms: PPARγ1 and PPARγ2. PPARγ1 is abundantly expressed in several tissues, whereas PPARγ2 is expressed mainly in adipose tissue (4). When a

* P. H. Bisschop and N. Bravenboer contributed equally to this work.
Address for reprint requests and other correspondence: K. M. Beekman, PO Box 7057, 1007 MB Amsterdam, The Netherlands (e-mail: k.beekman@vumc.nl).

ligand binds to PPARγ, a heterodimer is formed with retinoid X receptor-α, and this complex binds to PPARγ-responsive elements in the promotor regions of downstream PPARγ genes to initiate adipogenesis and regulate lipid metabolism and insulin sensitivity (33). PPARγ activation can modulate SCC fate resulting in stimulation of adipogenesis and inhibition of osteoblastogenesis and could play a key role in the BMAT increase and bone volume decrease seen with aging and in postmenopausal osteoporosis (11, 20). Therefore, inhibition of PPARγ seems a logical approach to prevent marrow adiposity and bone loss after menopause.

Previous animal studies have shown inconsistent effects of PPARγ modulation on bone and BMAT after ovariectomy. In PPARγ haploinsufficient mice, bone loss after ovariectomy was not different from wild-type animals (5). Mice overexpressing PPARγ specifically in osteoblasts showed accelerated bone loss after ovariectomy compared with wild-type ovariectomized mice (10). Another study showed that the PPARγ antagonist bisphenol A diglycidyl ether (BADGE) could return ovariectomy-induced marrow adiposity to sham levels in rats; however, BADGE had no effect on bone turnover or bone volume during estrogen deficiency (24). As BADGE binds PPARγ reversibly and has relatively low affinity and solubility, it is possible that BADGE had difficulty in achieving complete PPARγ antagonism (36, 46). Furthermore, some studies report PPARγ agonistic activity of BADGE (8, 28). A study by Sato et al. (35) showed that a different PPARγ antagonist could inhibit marrow adiposity. This group used GW9662, a potent PPARγ antagonist, which binds irreversibly to PPARγ. The effects of GW9662 on bone volume, bone quality, bone turnover, and BMAT during estrogen deficiency have not been described so far. Studies on BMAT often use aged animals, as old animals have larger amounts of BMAT. However, aged C57BL/6 mice, for example, have little trabecular bone volume left in their metaphysis, which makes it harder to study BMAT and bone parameters at the same time. C3H/HeJ mice have four times higher BMAT compared with C57BL/6 at the age of 12 wk (37), which makes the C3H/HeJ mouse a good animal model to study BMAT and bone together. The aim of this study was to determine if the PPARγ antagonist GW9662 can prevent ovariectomy-induced marrow adiposity and bone loss in C3H/HeJ mice, which have relatively high BMAT.

MATERIAL AND METHODS

Animals. The experiment was evaluated and approved by the institutional animal care and use committee of the Vrije Universiteit Medical Center in Amsterdam (No. Endo 14-01). All procedures were performed according to local, national, and international guidelines and laws on experimental animal care. Reporting was performed according to the Animal Research: Reporting of In Vivo Experiments guidelines.

Forty 40 female, 12-wk-old, C3H/HeJ mice (stock: 000659; Jackson Laboratories) were randomly assigned to four treatment groups (n = 10/group). Animals were group housed, with a 12-h light-dark cycle and a room temperature of 21°C. Chow (2016 Teklad global 16% protein rodent diets, T.2016MI), and water were available ad libitum. Chow was formulated to exclude soybean, thus minimizing the presence of phytoestrogen in the diet. After 2 wk of acclimatization, all animals underwent surgery: 20 mice were ovariectomized (OVX; bilateral approach, isoflurane anesthesia, pain medication: buprenorphine 0.05 mg/kg sc on the day of surgery) and 20 mice underwent bilateral laparotomy (sham surgery). After a 1-wk recovery, intraperitoneal injections with either GW9662 1 $mg \cdot kg^{-1} \cdot day^{-1}$ (Sigma-Aldrich) in 10% DMSO or 10% DMSO (vehicle) were administered daily at 10 AM for 3 consecutive weeks (3, 35). Animals were weighed daily, and dosing was adjusted accordingly. On *days 21* and *27*, 10 mg/kg calcein (Sigma-Aldrich) were administered intraperitoneally. On *day 28*, animals were euthanized via CO_2 inhalation. Subcutaneous (interscapular) adipose tissue was sampled, frozen in liquid nitrogen, and stored at −80°C until RNA isolation. Uteri were weighted to confirm successful ovariectomy. Left tibiae, right tibiae, and left femora were fixated in 2% phosphate-buffered paraformaldehyde (pH 6.9) at 4°C for 24 h before further processing for histology and contrast-enhanced nanocomputed topography (CE-CT). Right femora were wrapped in saline-immersed gauzes and frozen at −20°C for mechanical testing. Analysis of the data was performed blinded for treatment group.

MicroCT and CE-CT image acquisition and analysis. After 24 h of fixation, right tibiae were first transferred to PBS and were thereafter transferred to a polyoxometalate (POM)-based contrast solution (35 mg of Hafnium-Wells Dawson POM per 1 ml PBS). Before POM staining, the distal ends of the bones were removed to allow better diffusion of the contrast agent into the bone marrow compartment. Samples were incubated in the contrast solution, at 4°C while shaking gently, for 48 h before CE-CT imaging (21). Similar acquisition and reconstruction settings were applied as described previously (21): briefly, we used a Phoenix NanoTom M (GE Measurement and Control solutions, Germany) at a voltage of 70 kV and a current of 60 μA, and a 0.2-mm aluminum filter was used to reduce beam hardening. The exposure time was 500 ms, and 2,400 images were acquired over 360° using the fast scan mode (frame averaging = 1; image skip = 0), resulting in a scanning time of 20 min. We scanned at a 2-μm isotropic voxel size.

For analyses if the bone structural parameters, we used an in-house developed semiautomated protocol for drawing the volumes of interest around the trabecular bone region in the proximal metaphysis starting directly underneath growth plate and covering a height of 1.2 mm distal to the growth plate. One tibia was excluded from CE-CT analysis due to damage to the proximal metaphysis. Primary outcomes parameters were as follows: BMAT volume fraction as a percentage of the tissue volume (total adipose tissue volume, %), BMAT volume fraction as a percentage of the marrow volume (marrow adipose tissue volume, %), adipocyte diameter (μm), adipocyte density (cells/mm^3), and bone volume fraction (%). Secondary outcome parameters were trabecular thickness (μm), trabecular number (1/mm), and trabecular separation (mm).

Cortical parameters and mineralization degree were also determined in the right tibiae using microCT (μCT 40; Scanco Medical, Brüttisellen, Switzerland). Scan settings were as follows: peak voltage: 55 kVp; electric current: 144 μA; spatial resolution: 15 μm; and scan integration time: 200 ms. Beam hardening effects were reduced using both an aluminum filter in the microCT scanner and a correction algorithm in the software. To separate cortical bone from the background, a threshold of 650 mg hydroxyapatite (HA/cm^3) was used. Cortical parameters (cortical area, cortical thickness, and cortical mineralization) were determined in a middiaphyseal volume of interest of starting 1 mm proximal of the tibio-fibular junction, extending 1 mm in the proximal direction. Morphometry was performed using the uct_evaluation program (V6.6; Scanco Medical). MicroCT analysis was performed according to Bouxein et al. (9).

Bone histomorphometry. After fixation, the undecalcified left tibiae were processed for methyl methacrylate (MMA) embedding. MMA (BDH Chemicals, Poole, UK) was supplemented with 20% dibutyl phtalate (Merck, Darmstadt, Germany), 8.0 g/l dibenzoyl peroxide (AKZO Nobel, Deventer, The Netherlands), and 22 ml/10 ml *N*,*N*-dimethyl-*p*-toluidine (Merck). Sections of 5-mm thickness were cut with a Leica Jung K Polycut microtome (Nussloch, Germany) and subsequent sections were stained with calcein blue (Sigma-Aldrich),

as described by van 't Hof et al. (43b), or tartrate-resistant acid phosphatase (TRAP). Images were acquired using a Nikon microscope (Eclipse E 800), equipped with a DS-U1 camera (Nikon) and NIS-Elements AR software (version 2.34; Nikon, Düsseldorf, Germany) at a ×40 magnification. Three sections of each staining were analyzed per animal. Measurements were performed in the secondary spongiosa of the proximal metaphysis. All histomorphometric measurements were performed according to the guidelines of the American Society of Bone and Mineral Research (14). Images were analyzed using open source software based on ImageJ (43b). Histomorphometric measurements included mineral apposition rate (μm/day), mineralizing surface (%), and bone formation rate ($\mu m^3 \cdot \mu m^{-2} \cdot day^{-1}$) measured in the in the calcein blue-stained sections and osteoclast surface (%) and osteoclast number (#/mm) measured in TRAP-stained sections.

Immunohistochemistry. After 24 h of fixation, left femora were decalcified for 2 wk using ethylenediamine tetraacetic acid (EDTA (10%, pH 7.2) and subsequently embedded in paraffin. To detect PPARγ protein expression in the bone, immunohistochemical staining was performed on 5-μm-thick sections, using a monoclonal Rabbit anti-mouse PPARγ antibody as primary antibody (no. 2435; Cell Signaling Technology; Ref. 3) in a concentration of 1:100 in PBS-Tween. The secondary antibody was a polyclonal goat anti rabbit (E0432; DAKO). Antigen retrieval was performed by incubation with DNAse (D4527; Sigma-Aldrich) for 15 min. Nonspecific binding was blocked by incubating the bone sections in normal goat serum for 1 h at room temperature. Visualization was performed by incubation with horseradish peroxidase-conjugated streptavidin (T20931; Invitrogen) and tyramide signal amplification (T20931; Invitrogen) followed by staining with AEC substrate (OO2007; Invitrogen). Images were acquired using a Nikon microscope (Eclipse E 800), equipped with a DS-U1 camera (Nikon) and NIS-Elements AR software (version 2.34; Nikon, Düsseldorf, Germany) at a ×40 magnification. Two sections per femur were analyzed. Measurements were performed in the secondary spongiosa of the distal metaphysis. A binary was set using a threshold in NIS elements AR software to determine the area of PPARγ-positive cells (PPARγ.Ar), this area was divided by either the tissue area (T.Ar) or the marrow area (Ma.Ar) to determine the area fraction of PPARγ-positive cells (PPARγ.Ar/T.Ar or PPARγ.Ar/Ma.Ar, respectively).

Mechanical testing. A three-point bending was performed using a computer controlled Servohydraulic Instron testing device (Instron). For mechanical testing, samples were stored in saline-soaked gauzes at −20°C after harvesting and thawed just before the tests. All mechanical tests were performed at room temperature. A three-point bending test was performed on right femora according to Jepsen et al. (19). An in-house build set-up was manufactured, which consists of two parallel supports, spaced 10 mm. The middle support, attached to the loading device, was able to move in a vertical direction. Middiaphysis preload of 0.5 N was applied to stabilize the bone. Subsequently an increasing force, with a displacement rate of 1 mm/min, was applied until failure. The stiffness (N/mm), maximum load (N), and maximum displacement (mm) were calculated from the load displacement curve.

After three-point bending, distal right femora were used for a compression test (34, 43) on the distal metaphysis of the femora to test for the properties of cancellous bone. Distal parts of the femora were embedded in cold curing methylmetacrylate (×60; HBM Benelux, Waalwijk, The Netherlands). An in-house developed mold, fitting the femoral condyles, was constructed an placed on top of the specimen. A preload of 0.5 N was applied to stabilize the sample; thereafter, an uniaxial load to failure was applied, with a displacement rate of 1 mm/min. The stiffness (N/mm), maximum load (N), and maximum displacement (mm) were calculated from the load displacement curve.

RT-qPCR. One milliliter of cold TRI reagent was added to 50 mg of subcutaneous adipose tissue for RNA extraction. RNA isolation was performed by use of a RNA isolation kit (Macherey-Nagel, Düren, Germany), according to the manufacturer's protocol. RNA concentration was measured with a Nanodrop spectrophotometer (Nanodrop Technologies, Wilmington, DE). RNA was reverse transcribed from 100 ng total RNA in a 20-μl reaction mixture containing 5 mmol/l $MgCl_2$ (Eurogentec, Maastricht, The Netherlands); 1× RT buffer (Promega, Madison, WI); 1 mmol/l dATP, 1 mmol/l dCTP, 1 mmol/l dGTP, and 1 mmol/l dTTP (Roche Diagnostics, Mannheim, Germany); and 1 mmol/l betaïne, 10 ng/μl random primer, 0.4 U/μl RNAsin, and 5 U/μl M-MLV RT-enzyme (Promega), as described previously (43a). The PCR reaction was performed on a total volume of 25 μl, which contained 3 μl cDNA and 300 nmol/l reverse and forward primer and SYBR Green Supermix (Bio-Rad Laboratories, Veenendaal, The Netherlands). Downstream PPARγ genes glucose transporter 4 (*Glut 4*), Lipoprotein lipase (*LPL*), and fatty acid binding protein (*aP2*) were quantified. Primers are shown in Table 1. The PCR was performed on an iCycler iQTM Real-Time PCR Detection System (Bio-Rad): 3 min at 95°C, 40 cycles consisting of 15 s at 95°C and 1 min at 60°C. The relative gene expression was calculated by the $2^{-\Delta Ct}$ method, and *Beta-Actin* and *Beta2-microglobulin* were used as reference genes (primer sequences are shown in Table 1). Values >0.75 SD of the mean of the triplicate measurement were considered outliers and were excluded.

Statistics. This study was powered to detect a difference in BMAT volume fraction of 3% with a variance of 6%. The sample size was calculated using nQuery Advisor (Version 7.0) and power analysis was approved by the ethics committee of the Vrije Universiteit Medical Center. IBM SPSS Statistics for Windows (version 22; SPSS, Chicago, IL) was used for statistical analysis. Graphs were constructed using Graphpad Prism (Version 7.0 for Windows; GraphPad Software, La Jolla, CA). Means ± SD or median and interquartile ranges are reported, depending on the distribution of the data. The linear mixed model (LMM) was used to analyze the repeated weight measurements between the four groups. Based on the Akaike's Information Criterion and the Schwarz's Bayesian Criterion, first order autoregressive covariance structure was chosen. Two-way ANOVA was used to assess the effects of surgery and treatment and their interaction on the outcome parameters. The residuals were plotted to check their distribution. Levene's test was applied to check for homogeneity of variance. If either one of the assumptions was violated, the outcome parameter was rank transformed. All statistical tests were two sided, and $P = 0.05$ was considered statistically significant.

RESULTS

Body weight increased during the study in all groups (LMM, $P < 0.001$; Fig. 1). The increase in body weight was significantly larger in ovariectomized animals compared with sham-

Table 1. *Primers used for quantitative real-time PCR*

Gene	Forward Primer	Reverse Primer
β-Actin	AACCGTGAAAAGATGACCCAGAT	CACAGCCTGGATGGCTACGTA
β2-microglobulin	TGACCGGCTTGTATGCTATC	CAGTGTGAGCCAGGATATAG
Glut4	CAGCGCCTGAGTCTTTTCTT	GGCATTGATAACCCCAATGT
Lpl	CCCTAAGGACCCCTGAAGAC	GGCCCGATACAACCAGTCTA
aP2	ACACCGAGATTTCCTTCAAACTG	CCATCTAGGGTTATGATGCTCTTCA

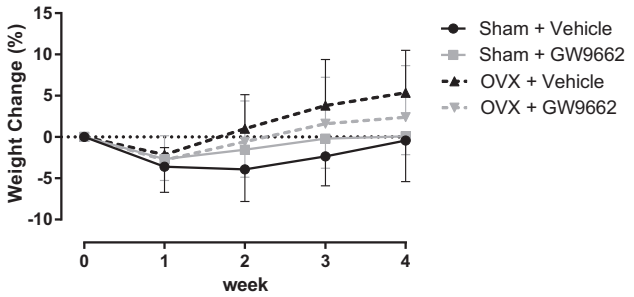

Fig. 1. Changes in body weight (%). In all groups (n = 10/group) body weight increased (LMM: $P < 0.001$). Body weight increased more in ovariectomized (OVX) mice compared with sham-operated mice (LMM: $P = 0.002$). GW9662 had no effect on body weight. Data are presented as median and interquartile range.

operated animals (LMM, $P = 0.002$). The PPARγ antagonist GW9662 did not affect weight changes. Uterine weight was lower in the ovariectomized animals [mean uterine weight OVX: 22 mg (SD 8) vs. sham 96 mg (SD 26); two-way ANOVA: $P < 0.001$], confirming estrogen deficiency. There was no effect of GW9662 on uterine weight (data not shown).

Bone marrow adipose tissue. Figure 2 shows a typical example of BMAT quantification using CE-CT. BMAT volume fraction, adipocyte size and adipocyte density were increased after 4 wk of ovariectomy compared with sham surgery (total adipose tissue volume: $P < 0.001$; marrow adipose tissue volume: $P < 0.001$; adipocyte diameter: $P = 0.001$; and adipocyte density: $P = 0.032$, respectively). GW9662 had no effect on either of the BMAT parameters and no interaction effects were found (Fig. 3*A*).

Bone structural parameters and bone turnover. Bone volume fraction, trabecular number, and average trabecular thickness were decreased after ovariectomy (bone volume fraction: $P < 0.001$; trabecular number: $P < 0.001$; trabecular thickness: $P < 0.001$; Fig. 3*B*), while there was no effect of GW9662. Trabecular separation increased after ovariectomy (trabecular separation: $P = 0.019$). We observed a significant interaction between ovariectomy and GW9662 (OVX*GW9662: $P = 0.029$): in sham-operated animals GW9662 increased the average trabecular separation, while in the ovariectomized animals GW9662 decreased the average trabecular separation (Fig. 3*B*). Representative images of the calcein labels and the TRAP staining are shown in Fig. 4. Mineralizing surface tended to increase after GW9662, both in ovariectomized and in sham-operated animals ($P = 0.066$), while there was no effect of OVX (Fig. 3*C*). Mineral apposition rate, bone formation, osteoclast surface, and osteoclast number (#/mm, data not shown) were not affected by OVX nor by GW9662 (Fig. 3*C*). Cortical area, cortical thickness, and cortical mineralization were not affected by either OVX or by GW9662 (data not shown).

PPARγ immunohistochemical staining. Immunohistochemical staining of the femora showed clear PPARγ protein expression in the bone marrow (Fig. 5*A*). There was no effect on of either treatment or surgery on the PPARγ stained area of the bone marrow, not when the PPARγ stained area was expressed as a percentage of the tissue area (PPARγ.Ar/T.Ar, data not shown), nor when the PPARγ-stained area was expressed as percentage of the marrow area (PPARγ.Ar/Ma.Ar, Fig. 5*B*).

Mechanical properties. OVX and GW9662 had no effect on maximum load or stiffness on the three-point bending test, but

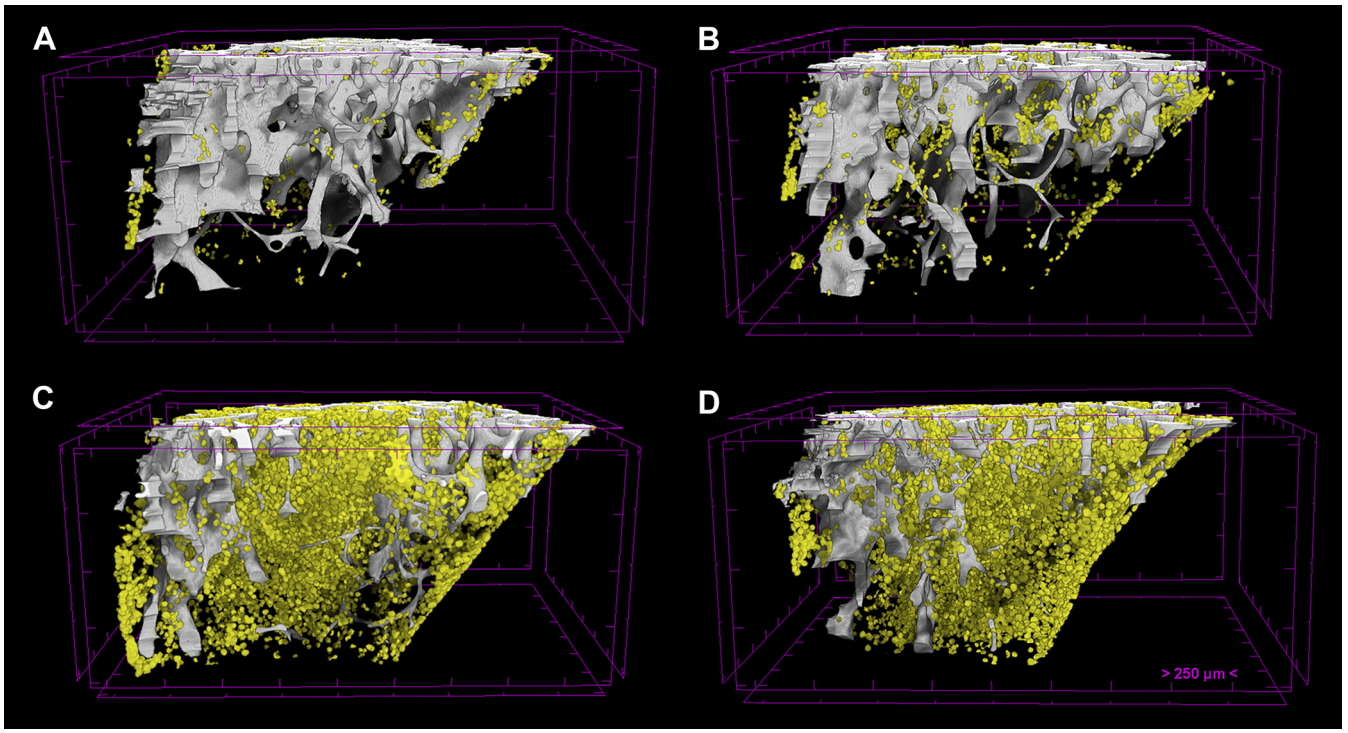

Fig. 2. 3-Dimensional quantification of bone marrow adipose tissue (yellow) in the proximal tibia using nanocomputed topography with a polyoxometalate-based contrast solution. Representative images of Sham + Vehicle (*A*), Sham + GW9662 (*B*), ovariectomy (OVX) + Vehicle (*C*), and OVX + GW9662 (*D*).

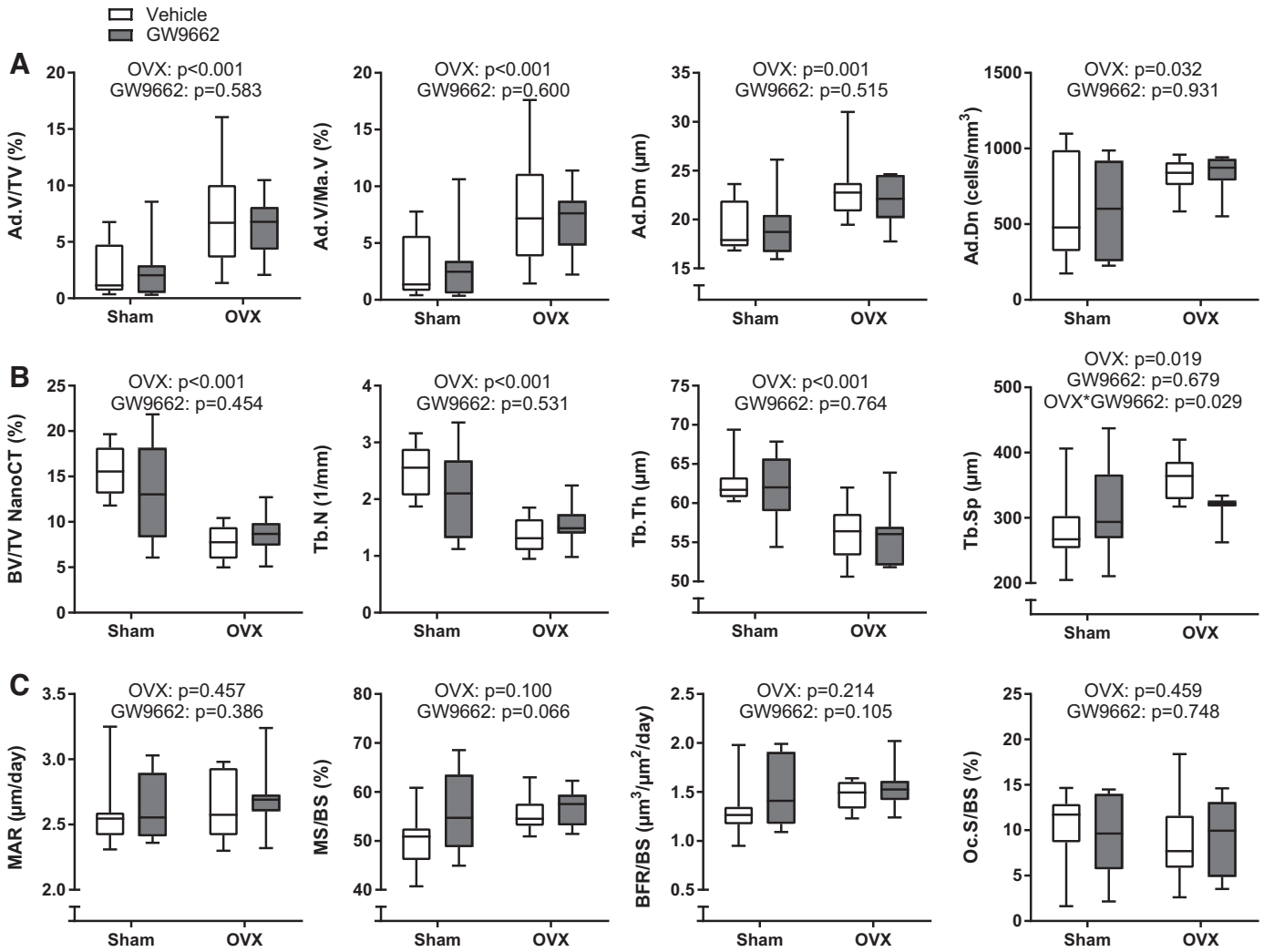

Fig. 3. *A*: bone marrow adipose tissue (BMAT) volume fraction (Ad.V/TV and Ad.V/Ma.V), adipocyte size (Ad.Dm) and adipocyte number (Ad.Dn) increased after ovariectomy (OVX). *B*: bone volume fraction (BV/TV), trabecular number (Tb.N), and trabecular thickness (Tb.Th) decreased after OVX. Trabecular separation (Tb.Sp) increased after OVX. In the sham group Tb.Sp increased after GW9662 and in the OVX group trabecular separation decreased after GW9662. *C*: ovariectomy and GW9662 did not affect bone turnover [mineral apposition rate (MAR), bone formation rate (BFR/BS), and osteoclast surface (Oc.S/BS)], although mineralizing surface (MS/BS) tended to increase after GW9662 ($P = 0.066$). Effects of surgery and treatment were assessed by two-way ANOVA, and boxplots represent median, interquartile range, and minimum and maximum values; $n = 10$/group, except for BMAT parameters in OVX + Veh group: $n = 9$.

GW9662 reduced maximum deformation ($P = 0.020$; Fig. 6*A*). Maximum load in the compression test was significantly lower after ovariectomy ($P < 0.001$). Stiffness in the compression test was not affected by OVX nor by GW9662. Maximum deformation tended to decrease after GW9662 in both sham and OVX animals ($P = 0.074$; Fig. 6*B*).

Subcutaneous adipose tissue. Glut4 expression in subcutaneous adipose tissue was increased after both OVX and

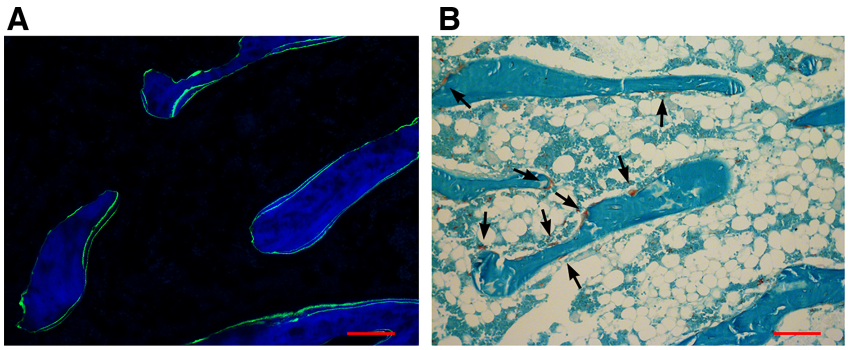

Fig. 4. *A*: calcein labels in the proximal metaphysis of the tibia, counterstained with calcein blue (×100 magnification). *B*: tartrate-resistant acid phosphatase staining showing osteoclasts, indicated by black arrows (×100 magnification). Scale bars = 100 µm.

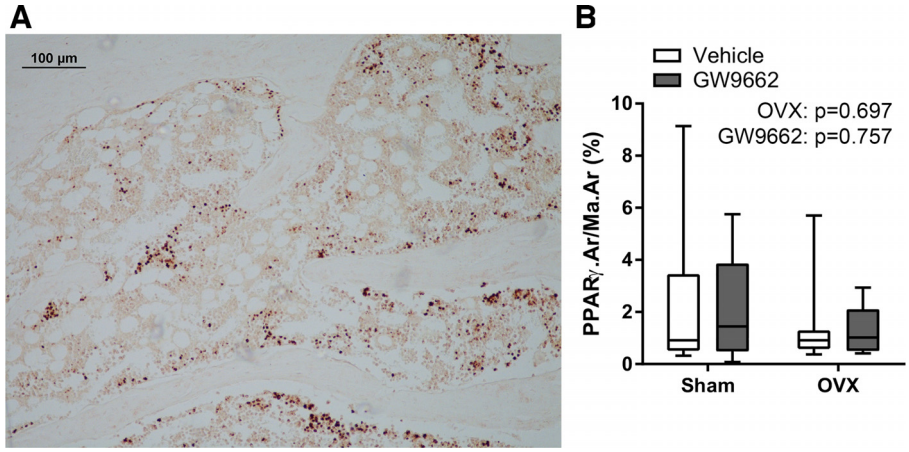

Fig. 5. *A*: immunohistochemical staining of including peroxisome proliferator-activated receptor-γ (PPARγ) in de distal metaphysis of the femur (magnification: ×100). *B*: PPARγ stained area was not affected by treatment nor by surgery. No interaction effects were found. Effects of surgery and treatment were assessed by two-way ANOVA, and boxplots represent median, interquartile range, and minimum and maximum values; $n = 10$/group, except for ovariectomy (OVX) + Veh: $n = 9$.

GW9662 (OVX: $P = 0.002$ and GW9662: $P = 0.013$; Fig. 7*A*). The same pattern was seen for *aP2* expression (OVX: $P = 0.003$ and GW9662: $P = 0.038$; Fig. 7*C*). *LPL* expression increased after OVX ($P = 0.004$) and showed a trend for an interaction effect (OVX*GW9662: $P = 0.059$): in sham animals GW9662 treatment tended to cause a higher expression of *LPL*, and in ovariectomized animals GW9662 tended to lower the expression of *LPL* (Fig. 7*B*).

DISCUSSION

Our study shows that systemic administration of the PPARγ antagonist GW9662 does not prevent high bone marrow adiposity and low bone volume after ovariectomy in C3H/HeJ mice. Our results oppose the current dogma that PPARγ promotes adipogenesis and inhibits osteoblastogenesis, but other studies on the effect of PPARγ on BMAT and bone metabolism have also shown unexpected effects (1, 5, 10, 24, 35).

Our results indicate that 3 wk of treatment with the PPARγ antagonist GW9662 does not decrease BMAT in C3H/HeJ mice. A previous study using the same compound to inhibit PPARγ showed a dramatic decrease in BMAT after 2 wk in a mouse model of aplastic anemia (35). The inconsistency with our results was unexpected as we used the same compound and dosage scheme. Possible explanations for the lack of effect of

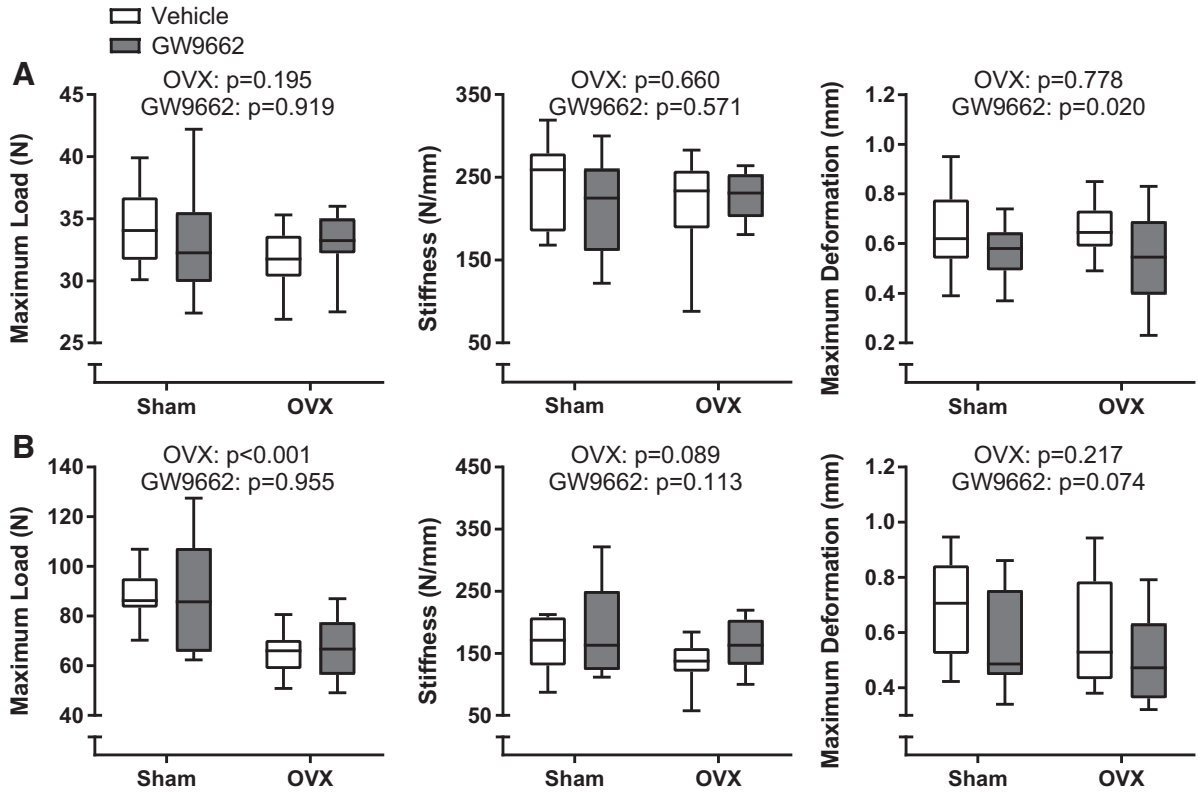

Fig. 6. *A*: 3-point bending test: maximum load and stiffness were not affected by ovariectomy (OVX) nor by GW9662. Maximum deformation decreased after GW9662 treatment ($P = 0.020$). *B*: compression test: maximum load was decreased after OVX; stiffness was not affected by OVX nor by GW9662; maximum deformation tended to decrease after GW9662 ($P = 0.074$). Effects of surgery and treatment were assessed by two-way ANOVA, and boxplots represent median, interquartile range, and minimum and maximum values; $n = 10$/group.

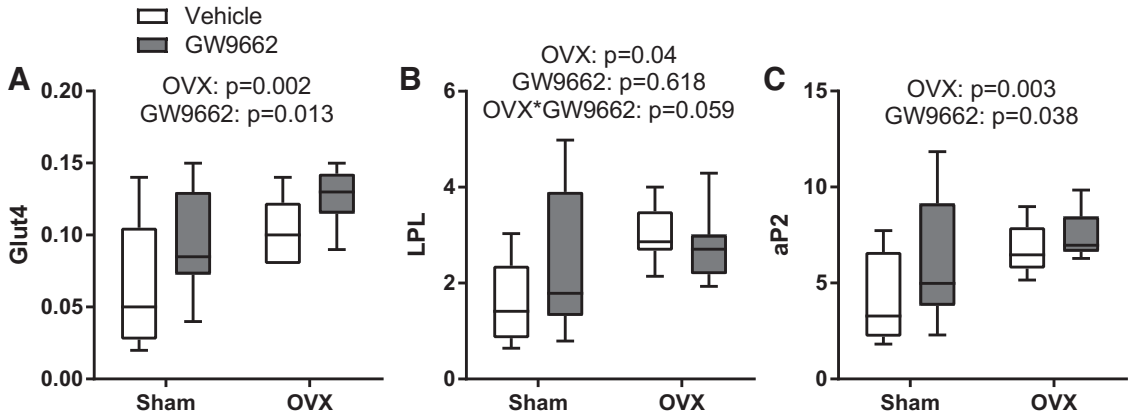

Fig. 7. *A* and *C*: relative mRNA expression of *Glut4* (*A*) and *aP2* (*C*) increased after ovariectomy and GW9662. *B*: *LPL* expression increased after ovariectomy (OVX) and GW9662 tended to increase *LPL* expression in the sham group and tended to decrease *LPL* expression in the OVX group (OVX*GW9662: $P = 0.059$). Effects of surgery, treatment, and interaction effects were assessed by two-way ANOVA, and boxplots represent median, interquartile range, and minimum and maximum values; $n = 10$/group.

GW9662 on BMAT in our study could be *1*) the genetic background of the mouse strain (which we will discuss in detail later), *2*) the different stimulus used to induce BMAT (aplastic anemia vs. ovariectomy in our study) and *3*) the timing of treatment initiation (1 day before the experiment vs. 1 wk of recovery after surgery in our study). It is important to consider that PPARγ antagonism is hypothesized to induce cell fate decisions of the SSC and therefore PPARγ antagonists might not be able to reverse already existing increases in adipose tissue when treatment is initiated after the causative event, but it could very well prevent increases in adiposity when treatment is initiated together with the causative event. However, it is unlikely that the total increase of BMAT we observed in the ovariectomized animals had already occurred within the first week after ovariectomy; this would leave opportunities for GW9662 to block the increase in BMAT in the second to fourth week after ovariectomy.

We show PPARγ protein expression within the bone marrow by immunohistochemical staining, which is a prerequisite for inducing an effect of a PPARγ antagonist. However, no effect of ovariectomy nor of GW9662 was seen on the distribution of PPARγ protein expression within the bone marrow, which indicates it has no significant role in bone marrow adipogenesis in C3H/HeJ mice. To confirm sufficient systemic exposure to GW9662 in our experiment, we determined gene expression downstream of PPARγ signaling in subcutaneous adipose tissue. GW9662 indeed changed the expression of PPARγ target genes. Interestingly, GW9662 is supposed to act as a PPARγ antagonist, but we observed increased adipocyte gene expression, indicating the effects of GW9662 were equivocal for all the targets examined and not only for bone marrow adipose tissue. It could be hypothesized that GW9662 can have both antagonistic and agonistic properties depending on the fat depot (BMAT vs. subcutaneous adipose), possibly through its PPARα agonistic activity (36, 40).

The current study shows that GW9662 has no effect on bone turnover, bone volume, and trabecular number or thickness, but it decreases maximum deformation on the three-point bending test in both sham and ovariectomized animals. As other cortical parameters, such as cortical mineralization and cortical thickness, are alike in all groups, the implications of the effect of GW9662 on maximum deformation are probably limited. This is consistent with a previous report showing that PPARγ haploinsufficiency ($PPAR\gamma^{+/-}$) does not affect ovariectomy induced bone loss (5). However, data on bone turnover in this study differed from our results as both $PPAR\gamma^{+/-}$ and wild-type animals showed increased bone turnover after ovariectomy while in our study bone turnover was not affected by either ovariectomy nor by GW9662. Possibly, the timing after OVX in our study (4 wk) is on the point of change of the initial high turnover phase right after OVX and the lower bone turnover phase later after ovariectomy. The lack of effect of ovariectomy and GW9662 on bone turnover could also be a power issue as histomorphometric measurements show relatively large variations in the measurements (13, 43b). On the other hand, in a genetic mouse model of increased PPARγ action (osteoblast specific overexpression of PPARγ), bone loss was accelerated following ovariectomy compared with wild-type mice (10). Again, all three studies differed in mouse strains used, timing of the measurements, and age of the animals. Furthermore, it could be postulated that genetic modifications in PPARγ expression might have different effects on bone metabolism than pharmacological PPARγ antagonists, as PPARγ also has ligand-independent basal activity of the receptor itself and ligand-dependent effects without specific binding to the DNA (15, 30). Finally, genetic modifications are already present at gestation whereas the pharmacological treatment begins later in life.

Since the abovementioned studies only considered the effects of PPARγ on either BMAT or on bone metabolism, it is difficult to compare studies directly. We showed that GW9662 has no effect on BMAT or bone parameters, with the exception of an interaction effect on trabecular separation: in estrogen-sufficient animals GW9662 increased trabecular separation, while in estrogen-deficient animals GW9662 decreased trabecular separation, suggesting a mild positive effect of GW9662 on bone in estrogen-deficient animals. However, as no similar patterns were observed for the other trabecular parameters, the implications of these findings are probably limited. In a study by Li et al. (24), with the use of BADGE to antagonize PPARγ action, BMAT decreased after BADGE, both in sham-operated and in ovariectomized Wistar rats), while improvement in bone

structural parameters and biomechanical competence after BADGE was only observed in sham-operated but not in ovariectomized rats. BADGE had no effect on bone turnover during estrogen deficiency, while BADGE increased bone formation during estrogen sufficiency (24). Together these results could indicate that the regulation of BMAT by PPARγ might be different during estrogen sufficiency and estrogen deficiency. An interaction between estrogen and PPARγ has not been described before, although estrogen is known to decrease PPARγ expression in bone marrow stem cells (16).

Methodological differences could account for the differences in the results between our study and the study by Li et al. (24). Animal strain differs (C3H/HeJ mice vs. Wistar rats), duration of the treatment differs (3 vs. 12 wk) and age of the animals is different (18 wk vs. 8 mo). It is conceivable that the interaction between marrow adipocytes and bone metabolism is different in old compared with younger animals. For example, PPARγ haploinsufficient (PPARγ$^{+/-}$) mice, 8 wk old, have similar BMAT as wild-type mice, while at 52 wk of age BMAT was decreased in PPARγ$^{+/-}$ animals compared with wild type. Bone volume was higher in PPARγ$^{+/-}$ mice both at 8 wk of age and at 52 wk of age (5). Differences could also be related to the compounds used. BADGE has potential PPARγ agonistic effects (8, 28), and it binds reversible to PPARγ (36). GW9662, on the other hand, binds irreversibly to PPARγ (23, 36). Some of the effects of GW9662 or lack thereof might by specific to the C3H/HeJ mouse. For instance, rosiglitazone treatment is an established method to induce BMAT, but 8 wk of rosiglitazone treatment in the C3H/HeJ mouse did not affect BMAT volume and decreased bone volume, as opposed to C57BL/6J mice in which bone volume remained unchanged and BMAT volume increased (1). Furthermore, it is possible that different expression patterns of PPARγ between animal strains cause differential effects of PPARγ in different animal strains. Lee et al. (22) showed that C3H/HeJ mice had nearly absent PPARγ protein and RNA in the liver, while C57BL/6 mice had abundant PPARγ in the liver. However, we show ample expression of PPARγ within the bone marrow of our C3H/HeJ mice.

We selected the C3H/HeJ mice as model because C3H/HeJ mice have four times more BMAT compared with C57BL/6 at the age of 12 wk (37). Generally, the larger the animal model, the more BMAT they have. Humans have more BMAT than rabbits and rabbits have more BMAT than mice (37). Mouse models like C57BL/6 have low BMAT volumes at a young age, and as BMAT increases with age, old animals would be preferred for studying BMAT. Unfortunately, aged C57BL/6 mice have little trabecular bone volume left, and thus changes in bone volume would be difficult to detect. As C3H/HeJ mice have both sufficient BMAT and sufficient bone volume at a relatively younger age, we chose this mouse as our model. The C3H/HeJ mice harbor a spontaneous missense mutation in the fourth exon of the Toll-like receptor 4 (*Tlr4*) gene (*Tlr4*$^{Lps\text{-}d}$) (32) causing loss of function of TLR4. The TLR4 pathway is part of the innate immune system; it increases T cells, which can produce receptor activator of nuclear factor-κB ligand (RANKL) (44) and thus cause an increase in osteoclasts. In C3H/HeJ mice, defective TLR4 signaling could explain the high bone density phenotype of C3H/HeJ mice caused by decreased osteoclasts (6). On the other hand, defective TLR4 signaling could lead to increased PPARγ expression (29) and thus cause the high BMAT phenotype of the C3H/HeJ mice; however, this does not fully explain the lack of effect of the PPARγ antagonist GW9662 in C3H/HeJ mice observed in our study.

In conclusion, the PPARγ antagonist GW9662 does not prevent high bone marrow adiposity and low bone volume after ovariectomy in C3H/HeJ mice, suggesting that BMAT accumulation is regulated independently of PPARγ in C3H/HeJ mice.

ACKNOWLEDGMENTS

We thank the biotechnical workers at the Universitair Proefdiercentrum Animal Facility at the Vrije Universiteit Medical Center, Huib van Essen, Ina Kamphuis, Mirjam Bethlehem, Kahin Abdelaziz, and Marleen Zwaagstra for excellent technical support at the Research Laboratory Bone and Calcium Metabolism at Vrije Universiteit Medical Center; Susanne LaFleur, Khalid Lamuadni and Unga Unmehopa for help with the RNA isolation at the Laboratory of Endocrinology at the Amsterdam University Medical Center; and Carla Geeroms and Sébastien de Bournonville for help with the contrast-enhanced nanocomputed topography image acquisition and analysis at KU Leuven.

GRANTS

K. M. Beekman is supported by an Alliancegrant provided by Vrije Universiteit Medical Center and Academic Medical Center/University of Amsterdam (2013-01). The contrast-enhanced nanocomputed topography images have been generated at the X-ray computed tomography facilities of the Department of Development and Regeneration of the KU Leuven, financed by the Hercules Foundation (Project AKUL 13/47).

DISCLAIMERS

Funding sources had no influence on the study design, the interpretation of the results, or the manuscript.

DISCLOSURES

No conflicts of interest, financial or otherwise, are declared by the authors.

AUTHOR CONTRIBUTIONS

K.M.B., P.H.B., and N.B. conceived and designed research; K.M.B. and A.v.d.V. performed experiments; K.M.B., A.v.d.V., and G.K. analyzed data; K.M.B., A.G.V.-V., P.H.B., and N.B. interpreted results of experiments; K.M.B. prepared figures; K.M.B. drafted manuscript; A.G.V.-V., M.M., G.K., P.H.B., and N.B. edited and revised manuscript; K.M.B., A.G.V.-V., A.v.d.V., M.d.H., M.M., G.K., T.N.P.-V., P.H.B., and N.B. approved final version of manuscript.

REFERENCES

1. **Ackert-Bicknell CL, Shockley KR, Horton LG, Lecka-Czernik B, Churchill GA, Rosen CJ.** Strain-specific effects of rosiglitazone on bone mass, body composition, and serum insulin-like growth factor-I. *Endocrinology* 150: 1330–1340, 2009. doi:10.1210/en.2008-0936.
3. **Ahmad I, Mui E, Galbraith L, Patel R, Tan EH, Salji M, Rust AG, Repiscak P, Hedley A, Markert E, Loveridge C, van der Weyden L, Edwards J, Sansom OJ, Adams DJ, Leung HY.** Sleeping Beauty screen reveals Pparg activation in metastatic prostate cancer. *Proc Natl Acad Sci USA* 113: 8290–8295, 2016. doi:10.1073/pnas.1601571113.
4. **Ahmadian M, Suh JM, Hah N, Liddle C, Atkins AR, Downes M, Evans RM.** PPARγ signaling and metabolism: the good, the bad and the future. *Nat Med* 19: 557–566, 2013. doi:10.1038/nm.3159.
5. **Akune T, Ohba S, Kamekura S, Yamaguchi M, Chung UI, Kubota N, Terauchi Y, Harada Y, Azuma Y, Nakamura K, Kadowaki T, Kawaguchi H.** PPARgamma insufficiency enhances osteogenesis through osteoblast formation from bone marrow progenitors. *J Clin Invest* 113: 846–855, 2004. doi:10.1172/JCI200419900.
6. **Amblard D, Lafage-Proust MH, Chamson A, Rattner A, Collet P, Alexandre C, Vico L.** Lower bone cellular activities in male and female mature C3H/HeJ mice are associated with higher bone mass and different pyridinium crosslink profiles compared to C57BL/6J mice. *J Bone Miner Metab* 21: 377–387, 2003. doi:10.1007/s00774-003-0432-8.

7. **Beekman KM, Veldhuis-Vlug AG, den Heijer M, Maas M, Oleksik AM, Tanck MW, Ott SM, van 't Hof RJ, Lips P, Bisschop PH, Bravenboer N.** The effect of raloxifene on bone marrow adipose tissue and bone turnover in postmenopausal women with osteoporosis. *Bone*, 118: 62–68, 2019. doi:10.1016/j.bone.2017.10.011.
8. **Bishop-Bailey D, Hla T, Warner TD.** Bisphenol A diglycidyl ether (BADGE) is a PPARgamma agonist in an ECV304 cell line. *Br J Pharmacol* 131: 651–654, 2000. doi:10.1038/sj.bjp.0703628.
9. **Bouxsein ML, Boyd SK, Christiansen BA, Guldberg RE, Jepsen KJ, Müller R.** Guidelines for assessment of bone microstructure in rodents using micro-computed tomography. *J Bone Miner Res* 25: 1468–1486, 2010. doi:10.1002/jbmr.141.
10. **Cho SW, Yang JY, Her SJ, Choi HJ, Jung JY, Sun HJ, An JH, Cho HY, Kim SW, Park KS, Kim SY, Baek WY, Kim JE, Yim M, Shin CS.** Osteoblast-targeted overexpression of PPARγ inhibited bone mass gain in male mice and accelerated ovariectomy-induced bone loss in female mice. *J Bone Miner Res* 26: 1939–1952, 2011. doi:10.1002/jbmr.366.
11. **Cohen A, Dempster DW, Stein EM, Nickolas TL, Zhou H, McMahon DJ, Müller R, Kohler T, Zwahlen A, Lappe JM, Young P, Recker RR, Shane E.** Increased marrow adiposity in premenopausal women with idiopathic osteoporosis. *J Clin Endocrinol Metab* 97: 2782–2791, 2012. doi:10.1210/jc.2012-1477.
12. **Colditz GA, Hankinson SE, Hunter DJ, Willett WC, Manson JE, Stampfer MJ, Hennekens C, Rosner B, Speizer FE.** The use of estrogens and progestins and the risk of breast cancer in postmenopausal women. *N Engl J Med* 332: 1589–1593, 1995. doi:10.1056/NEJM199506153322401.
13. **Compston JE, Vedi S, Stellon AJ.** Inter-observer and intra-observer variation in bone histomorphometry. *Calcif Tissue Int* 38: 67–70, 1986. doi:10.1007/BF02556831.
14. **Dempster DW, Compston JE, Drezner MK, Glorieux FH, Kanis JA, Malluche H, Meunier PJ, Ott SM, Recker RR, Parfitt AM.** Standardized nomenclature, symbols, and units for bone histomorphometry: a 2012 update of the report of the ASBMR Histomorphometry Nomenclature Committee. *J Bone Miner Res* 28: 2–17, 2013. doi:10.1002/jbmr.1805.
15. **Feige JN, Gelman L, Michalik L, Desvergne B, Wahli W.** From molecular action to physiological outputs: peroxisome proliferator-activated receptors are nuclear receptors at the crossroads of key cellular functions. *Prog Lipid Res* 45: 120–159, 2006. doi:10.1016/j.plipres.2005.12.002.
16. **Gao B, Huang Q, Lin YS, Wei BY, Guo YS, Sun Z, Wang L, Fan J, Zhang HY, Han YH, Li XJ, Shi J, Liu J, Yang L, Luo ZJ.** Dose-dependent effect of estrogen suppresses the osteo-adipogenic transdifferentiation of osteoblasts via canonical Wnt signaling pathway. *PLoS One* 9: e99137, 2014 [Erratum in *PLoS One* 9: e114981, 2014]. doi:10.1371/journal.pone.0099137.
17. **Grady D, Rubin SM, Petitti DB, Fox CS, Black D, Ettinger B, Ernster VL, Cummings SR.** Hormone therapy to prevent disease and prolong life in postmenopausal women. *Ann Intern Med* 117: 1016–1037, 1992. doi:10.7326/0003-4819-117-12-1016.
18. **Griffith JF, Yeung DK, Antonio GE, Wong SY, Kwok TC, Woo J, Leung PC.** Vertebral marrow fat content and diffusion and perfusion indexes in women with varying bone density: MR evaluation. *Radiology* 241: 831–838, 2006. doi:10.1148/radiol.2413051858.
19. **Jepsen KJ, Silva MJ, Vashishth D, Guo XE, van der Meulen MC.** Establishing biomechanical mechanisms in mouse models: practical guidelines for systematically evaluating phenotypic changes in the diaphyses of long bones. *J Bone Miner Res* 30: 951–966, 2015. doi:10.1002/jbmr.2539.
20. **Justesen J, Stenderup K, Ebbesen EN, Mosekilde L, Steiniche T, Kassem M.** Adipocyte tissue volume in bone marrow is increased with aging and in patients with osteoporosis. *Biogerontology* 2: 165–171, 2001. doi:10.1023/A:1011513223894.
21. **Kerckhofs G, Stegen S, van Gastel N, Sap A, Falgayrac G, Penel G, Durand M, Luyten FP, Geris L, Vandamme K, Parac-Vogt T, Carmeliet G.** Simultaneous three-dimensional visualization of mineralized and soft skeletal tissues by a novel microCT contrast agent with polyoxometalate structure. *Biomaterials* 159: 1–12, 2018. doi:10.1016/j.biomaterials.2017.12.016.
22. **Lee YJ, Ko EH, Kim JE, Kim E, Lee H, Choi H, Yu JH, Kim HJ, Seong JK, Kim KS, Kim JW.** Nuclear receptor PPARγ-regulated monoacylglycerol O-acyltransferase 1 (MGAT1) expression is responsible for the lipid accumulation in diet-induced hepatic steatosis. *Proc Natl Acad Sci USA* 109: 13656–13661, 2012. doi:10.1073/pnas.1203218109.
23. **Leesnitzer LM, Parks DJ, Bledsoe RK, Cobb JE, Collins JL, Consler TG, Davis RG, Hull-Ryde EA, Lenhard JM, Patel L, Plunket KD, Shenk JL, Stimmel JB, Therapontos C, Willson TM, Blanchard SG.** Functional consequences of cysteine modification in the ligand binding sites of peroxisome proliferator activated receptors by GW9662. *Biochemistry* 41: 6640–6650, 2002. doi:10.1021/bi0159581.
24. **Li G, Xu Z, Hou L, Li X, Li X, Yuan W, Polat M, Chang S.** Differential effects of bisphenol A diglicydyl ether on bone quality and marrow adiposity in ovary-intact and ovariectomized rats. *Am J Physiol Endocrinol Metab* 311: E922–E927, 2016. doi:10.1152/ajpendo.00267.2016.
25. **Limonard EJ, Veldhuis-Vlug AG, van Dussen L, Runge JH, Tanck MW, Endert E, Heijboer AC, Fliers E, Hollak CE, Akkerman EM, Bisschop PH.** Short-term effect of estrogen on human bone marrow fat. *J Bone Miner Res* 30: 2058–2066, 2015. doi:10.1002/jbmr.2557.
26. **Lufkin EG, Wahner HW, O'Fallon WM, Hodgson SF, Kotowicz MA, Lane AW, Judd HL, Caplan RH, Riggs BL.** Treatment of postmenopausal osteoporosis with transdermal estrogen. *Ann Intern Med* 117: 1–9, 1992. doi:10.7326/0003-4819-117-1-1.
28. **Nakamuta M, Enjoji M, Uchimura K, Ohta S, Sugimoto R, Kotoh K, Kato M, Irie T, Muta T, Nawata H.** Bisphenol a diglycidyl ether (BADGE) suppresses tumor necrosis factor-α production as a PPARγ agonist in the murine macrophage-like cell line, RAW 264.7. *Cell Biol Int* 26: 235–241, 2002. doi:10.1006/cbir.2001.0838.
29. **Necela BM, Su W, Thompson EA.** Toll-like receptor 4 mediates cross-talk between peroxisome proliferator-activated receptor gamma and nuclear factor-kappaB in macrophages. *Immunology* 125: 344–358, 2008. doi:10.1111/j.1365-2567.2008.02849.x.
30. **Pascual G, Glass CK.** Nuclear receptors versus inflammation: mechanisms of transrepression. *Trends Endocrinol Metab* 17: 321–327, 2006. doi:10.1016/j.tem.2006.08.005.
31. **Pittenger MF, Mackay AM, Beck SC, Jaiswal RK, Douglas R, Mosca JD, Moorman MA, Simonetti DW, Craig S, Marshak DR.** Multilineage potential of adult human mesenchymal stem cells. *Science* 284: 143–147, 1999. doi:10.1126/science.284.5411.143.
32. **Poltorak A, He X, Smirnova I, Liu MY, Van Huffel C, Du X, Birdwell D, Alejos E, Silva M, Galanos C, Freudenberg M, Ricciardi-Castagnoli P, Layton B, Beutler B.** Defective LPS signaling in C3H/HeJ and C57BL/10ScCr mice: mutations in Tlr4 gene. *Science* 282: 2085–2088, 1998. doi:10.1126/science.282.5396.2085.
33. **Sadie-Van Gijsen H, Hough FS, Ferris WF.** Determinants of bone marrow adiposity: the modulation of peroxisome proliferator-activated receptor-γ2 activity as a central mechanism. *Bone* 56: 255–265, 2013. doi:10.1016/j.bone.2013.06.016.
34. **Sankar U, Pritchard ZJ, Voor MJ.** Micro-computed tomography assisted distal femur metaphyseal blunt punch compression for determining trabecular bone strength in mice. *J Biomech* 49: 1233–1237, 2016. doi:10.1016/j.jbiomech.2016.02.040.
35. **Sato K, Feng X, Chen J, Li J, Muranski P, Desierto MJ, Keyvanfar K, Malide D, Kajigaya S, Young NS.** PPARγ antagonist attenuates mouse immune-mediated bone marrow failure by inhibition of T cell function. *Haematologica* 101: 57–67, 2016. doi:10.3324/haematol.2014.121632.
36. **Schaefer KL.** PPARγ inhibitors as novel tubulin-targeting agents. *PPAR Res* 2008: 785405, 2008. doi:10.1155/2008/785405.
37. **Scheller EL, Doucette CR, Learman BS, Cawthorn WP, Khandaker S, Schell B, Wu B, Ding SY, Bredella MA, Fazeli PK, Khoury B, Jepsen KJ, Pilch PF, Klibanski A, Rosen CJ, MacDougald OA.** Region-specific variation in the properties of skeletal adipocytes reveals regulated and constitutive marrow adipose tissues. *Nat Commun* 6: 7808, 2015 [Erratum in *Nat Commun* 7: 13775, 2016]. doi:10.1038/ncomms8808.
38. **Schellinger D, Lin CS, Hatipoglu HG, Fertikh D.** Potential value of vertebral proton MR spectroscopy in determining bone weakness. *AJNR Am J Neuroradiol* 22: 1620–1627, 2001.
39. **Schwartz AV, Sigurdsson S, Hue TF, Lang TF, Harris TB, Rosen CJ, Vittinghoff E, Siggeirsdottir K, Sigurdsson G, Oskarsdottir D, Shet K, Palermo L, Gudnason V, Li X.** Vertebral bone marrow fat associated with lower trabecular BMD and prevalent vertebral fracture in older adults. *J Clin Endocrinol Metab* 98: 2294–2300, 2013. doi:10.1210/jc.2012-3949.
40. **Seimandi M, Lemaire G, Pillon A, Perrin A, Carlavan I, Voegel JJ, Vignon F, Nicolas JC, Balaguer P.** Differential responses of PPARalpha, PPARdelta, and PPARgamma reporter cell lines to selective PPAR synthetic ligands. *Anal Biochem* 344: 8–15, 2005. doi:10.1016/j.ab.2005.06.010.

41. **Syed FA, Oursler MJ, Hefferanm TE, Peterson JM, Riggs BL, Khosla S.** Effects of estrogen therapy on bone marrow adipocytes in postmenopausal osteoporotic women. *Osteoporos Int* 19: 1323–1330, 2008. doi:10.1007/s00198-008-0574-6.
42. **Tencerova M, Kassem M.** The bone marrow-derived stromal cells: commitment and regulation of adipogenesis. *Front Endocrinol (Lausanne)* 7: 127, 2016. doi:10.3389/fendo.2016.00127.
43. **Turner CH, Burr DB.** Basic biomechanical measurements of bone: a tutorial. *Bone* 14: 595–608, 1993. doi:10.1016/8756-3282(93)90081-K.
43a. **van der Meijden K, Buskermolen J, van Essen HW, Schuurman T, Steegenga WT, Brouwer-Brolsma EM, Langenbach GEJ, van Ruijven LJ, den Heijer M, Lips P, Bravenboer N.** Long-term vitamin D deficiency in older adult C57BL/6 mice does not affect bone structure, remodeling and mineralization. *J Steroid Biochem Mol Biol* 164: 344–352, 2016. doi:10.1016/j.jsbmb.2015.09.004.
43b. **van 't Hof RJ, Rose L, Bassonga E, Daroszewska A.** Open source software for semi-automated histomorphometry of bone resorption and formation parameters. *Bone* 99: 69–79, 2017. doi:10.1016/j.bone.2017.03.051.
44. **Walsh MC, Takegahara N, Kim H, Choi Y.** Updating osteoimmunology: regulation of bone cells by innate and adaptive immunity. *Nat Rev Rheumatol* 14: 146–156, 2018. doi:10.1038/nrrheum.2017.213.
45. **Wehrli FW, Hopkins JA, Hwang SN, Song HK, Snyder PJ, Haddad JG.** Cross-sectional study of osteopenia with quantitative MR imaging and bone densitometry. *Radiology* 217: 527–538, 2000. doi:10.1148/radiology.217.2.r00nv20527.
46. **Wright HM, Clish CB, Mikami T, Hauser S, Yanagi K, Hiramatsu R, Serhan CN, Spiegelman BM.** A synthetic antagonist for the peroxisome proliferator-activated receptor gamma inhibits adipocyte differentiation. *J Biol Chem* 275: 1873–1877, 2000. doi:10.1074/jbc.275.3.1873.